The Moisture Budget over the Northeastern Arabian Sea during Premonsoon and Monsoon Onset, 1979

MICHAEL R. HOWLAND[1] AND DHIRENDRA N. SIKDAR

Atmospheric Sciences, University of Wisconsin, Milwaukee, WI 53211

(Manuscript received 12 March 1983, in final form 9 August 1983)

ABSTRACT

Moisture budgets are calculated for premonsoon and monsoon onset conditions in the northeastern Arabian Sea during summer 1979 from kinematic analysis of aircraft dropsonde, ship and island radiosonde, and satellite-derived winds. Dramatic changes are observed between the premonsoon and monsoon onset mean kinematic and moisture fields. Specific humidity increased as much as 5 g kg^{-1} in much of the middle troposphere between 29 May and 17 June 1979. This is apparently due to deep convection during the monsoon onset period and mid-level advection of moisture during the premonsoon period. Flux of moisture through the budget boundaries is comparable to previous estimates for the Arabian Sea. It is shown that the loss of moisture through cirrus outflow accounts for only 1–3% of the total budget flux. Evaporation from the sea surface is 3 to 4 times higher during the onset period and was greatest south of 12°N. Maps of precipitation as a residual of the moisture budget computations agree remarkably well with convective features seen in satellite imagery. During the monsoon onset period, rainfall averaged about 1 mm h^{-1} over the entire budget area. In order to test the validity of the combined data base and moisture budget computations, two independent estimates of precipitation were made using a Krishnamurti *et al.* parameterization scheme and the Stout *et al.* satellite technique. Both showed good agreement to the budget results.

1. Introduction

Numerous investigations have been made into the meteorology of the Arabian Sea and the onset of the Indian summer monsoon. Much of the emphasis has been placed on the study of the wind circulation before and after the monsoon onset. The development of the Somali low-level wind jet and the strengthening of the easterly upper-level flow have been investigated to a considerable extent. Findlater (1969, 1971), Krishnamurti and Bhalme (1976), Krishnamurti *et al.* (1976), and Cadet and Desbois (1980) are just a few examples of the Somali jet studies. The effect of this flow is not only to transport moisture, but to increase the evaporation over the Arabian Sea as well (Pisharoty, 1965). The moisture flow over the Arabian Sea has an important relationship to the development of deep convection over the sea and the spread of convective rains onto the Indian continent during the monsoon season (Saha and Bavadekar, 1977). A detailed knowledge of the changes in the three-dimensional moisture distribution would be of extreme importance to monsoon forecasters and modelers. One way to examine this flow of moisture is through the use of a moisture budget.

Pisharoty (1965) used data collected by the International Indian Ocean Expedition (IIOE) of 1963–64 to compute a water budget in the volume 42 to 75°E and 0 to 26°N from the sea surface to 450 mb over the Arabian Sea. He concluded that the Indian summer monsoon picked up most of its moisture as evaporation from the Sea. Saha (1970), using additional equatorial sounding data, computed results for the same budget area/time period and found that the flux of water vapor across the equator amounted to 73.4% of the outflow across 75°E. This was in contrast with the earlier findings of Pisharoty. In an extension of his work, Saha and Bavadekar (1973) used the same data base, but added evaporation computed from the IIOE of 1963–64 to estimate precipitation as a residual of the moisture budget. Their results produced total budget area average precipitation which was comparable to amounts they estimated from available observed rainfall charts. Although these studies produced reasonable results on the large scale, no resolution of detail was possible with the limited data available.

For the 1973 monsoon season Ghosh *et al.* (1978) looked at moisture transport over the Arabian Sea during active and weak monsoon periods using June and July data from the INDO–USSR monsoon experiment of 1973. They found that cross-equatorial flux was not always the largest source of moisture crossing the 75°E meridian. In fact, during the active monsoon periods they found that this amounted to

[1] Current affiliation: Space Science and Engineering Center, University of Wisconsin, Madison 53706.

© 1983 American Meteorological Society

less than one half of the outflow across 75°E. This implied that Arabian sea evaporation was important during periods of active monsoon. During weak monsoon, their findings were similar to the monthly results of Saha (1970) and Saha and Bavadekar (1973).

More recently, Hastenrath and Lamb (1980) used 60 years of ship observations, wind fields at 850, 700 and 500 mb and available radiosonde data for specific humidity, to compute heat and moisture budgets over the Indian Ocean. They concluded that the flux of moisture across the equator was the dominant source of moisture for the coasts of southern Asia. Cadet (1981) and Cadet and Reverdin (1981) also examined the water vapor transport over the Indian Ocean. They studied the monsoon season of 1975 and found that 70% of the water vapor crossing the western coast of India came from the Southern Hemisphere. The remaining 30% was attributed to Arabian Sea evaporation. They also concluded that the region of 45–60°E accounted for over 50% of the total cross-equatorial flux of moisture.

In a slightly different approach, Rao *et al.* (1981) compared estimates of evaporation over the Arabian Sea to microwave satellite-derived rainfall estimates for the monsoon seasons of 1973, 1974 and 1977. The mean monthly evaporation was found to be maximum during June, and the total estimated precipitation over the Arabian Sea amounted to only 40% of the Arabian Sea evaporation during the summers of 1973 and 1974. The remaining moisture was hypothesized as being transported into India.

The studies mentioned above suggest that cross-equatorial flux of moisture provides the dominant source of moisture for the Indian summer monsoon. They have also shown that evaporation from the Arabian Sea is indeed significant. Both of these moisture sources are related to the strength of the low-level southwesterly flow. All of this previous work has been based on a limited data sample and has excluded the flux of moisture above 400 mb. In one case, (Hastenrath and Lamb, 1980) the upper bound was 500 mb. Additionally, they have been computed over a monthly or semimonthly time scale. The purpose of this study is to have a second look at moisture budget estimates over the Arabian Sea during premonsoon and monsoon onset conditions using data collected during the Monsoon Experiment of the FGGE year (1979). We have been able to sample the progression of the southwest (SW) monsoon circulation on a daily scale. This provides a closer and more detailed view than possible from previous studies.

2. Data

Data for use in the budget computations comes from a variety of sources and were collected during the Summer Monsoon Experiment (SMONEX), 1979. A summary of the Summer Monsoon Experiment scientific objectives, study phases, and data sources is written by Fein and Kuettner (1980). The data used in this budget study consists of aircraft dropsonde, island and coastal radiosonde, ship radiosonde, ship surface data, satellite-derived upper-level winds (used at the 200 mb level), and visible and infrared satellite imagery from GOES-IO. Availability of data, particularly the locations of aircraft dropsondes, was a factor in selecting the budget boundary. The budget area is shown in Fig. 1. The volume is defined from 60 to 72°E and from 6 to 18°N over the northeast Arabian Sea. The height of the volume extends from the approximate surface (1000 mb) to the approximate tropopause (100 mb). This area of 12° latitude by 12° longitude is well centered to study the effects of the low-level southwesterly jet as it transports moisture across the Arabian Sea. Fig. 1 displays the flight tracks, dropsonde locations, and radiosonde stations available for the 18 June budget. This day had the best data coverage of all days selected for the moisture budget computations.

The principal data for the moisture budget are the aircraft dropsondes contained in the FGGE Quick Look Data Set. This data set was used due to errors created and resulting delays in the production of a final FGGE level II-b dropsonde data set. Dropsonde data were subjected to considerable screening as discussed later. Radiosonde data from ships and island stations were obtained from computer tape of the FGGE level II-b data set. Satellite-derived winds (Young *et al.*, 1980) were used to represent 200 mb winds since dropsondes at best were available only to about 350 mb.

Surface temperatures and humidity data were obtained by compositing ship reports (FGGE II-b data) with dropsondes which terminated at pressures similar to those reported by the nearest ships. This was nec-

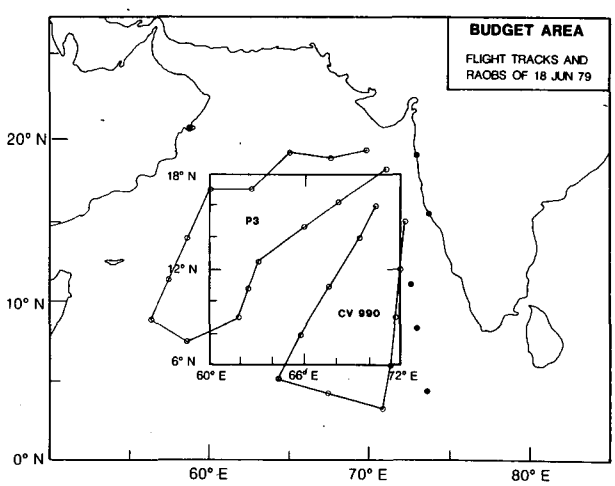

FIG. 1. The moisture budget area is shown by the 12° × 12° enclosed box. Island and coastal radiosonde stations are shown by the solid circles. Dropsonde locations are shown by open circles.

essary as neither data source gave adequate surface coverage when used alone (ship observations were only 8–14 per day and not evenly distributed in the budget area). This combined surface data was used to estimate surface evaporation. Dropsondes provided temperature and humidity data for the 1000 mb level, but typically did not report winds below 950 mb. Estimation of the 1000 mb winds will be covered later.

Visible and infrared satellite imagery were obtained (from the Space Science and Engineering Center, University of Wisconsin-Madison) at two mile resolution for 0730 and 0800 GMT on each day of the budget study. The satellite imagery was used to locate convective features, to compute cirrus outflow, and to compute satellite-estimated rainfall.

The sampling dates for this study were limited to the days when dropsonde coverage of the Arabian Sea was fairly extensive. The dates were chosen to be representative of the synoptic conditions typical to premonsoon and monsoon onset. They were also selected to be as close together as possible to emphasize the local change term in the moisture budget. The days 29 May and 3 June were chosen to represent premonsoon and 15, 17, and 18 June to represent monsoon onset. The latter set was chosen to follow as nearly after development of monsoon conditions as possible. This would emphasize the changes which occur over an approximate two week span.

3. Procedure

Data reduction involved both subjective and objective techniques. The dropsonde data were subjectively analyzed for obvious data errors. All sounding data were linearly interpolated to a vertical interval of 50 mb. Poor vertical resolution of the raw sounding data made interpolation finer than 50 mb impractical. The sounding data was screened a second time for errors after interpolation. Suspect values were discarded or manually interpolated both vertically and horizontally with the nearest soundings. About 95% of the original dropsonde data were retained.

Grid point values at 1° interval of latitude and longitude for u, v, and q were generated by objective analysis of the sounding data. Here u and v are westerly and southerly components of the horizontal wind, and q is specific humidity. Barnes' (1964) technique for objective analysis was utilized in a slightly modified form. The modification was to use a variable search radius as follows. Initial search radius was sufficiently large to include approximately 50% of all dropsonde and radiosonde data. Subsequently, the search radius was reduced to a final value of about 4½° latitude/longitude or 1.5 times the soundings average spacing. Ship as well as island and coastal radiosonde data were incorporated into the objective analysis when they were available. The initial large search radius was necessary to produce a fairly smooth initial data field. This prevented unreasonably large gradients from occurring when either the northwest or southwest corner of the budget area was "data poor". After objective analysis, the original data was overlayed on the gridded field to insure that a good fit occurred at the original data points. The resulting fields were good reproductions based on the original data.

The moisture parameters supplied in the raw dropsonde data were relative humidity and dewpoint temperature. Saturation vapor pressure was computed from the sounding temperature data as an intermediate step in deriving specific humidity. Lowe (1977) provides a polynomial approximation for e_s which was used to compute the vapor pressure (e) from the sounding reports of relative humidity. The vapor pressure and air pressure were then used to compute specific humidity.

The gridded fields of u and v allowed computation of grid point values of divergence. The vertical velocity in pressure coordinates was computed from the integration of the continuity equation:

$$\frac{\partial \omega}{\partial p} = -(\nabla \cdot \mathbf{V}). \tag{1}$$

After integration, the equation for vertical velocity at level p is

$$\omega_p = \omega_{p+\Delta p} + \int_p^{p+\Delta p} \left(\frac{\partial u}{\partial x} + \frac{\partial v}{\partial y}\right) dp. \tag{2}$$

A scheme to adjust the resultant vertical velocities to match the assumed boundary conditions (that $\omega = 0$ at $p = 100$ and 1000 mb) as shown by O'Brien (1970) and also outlined by Fankhauser (1969), was used to adjust the final kinematic vertical velocities. The three-dimensional grid point values were used to compute the moisture budget as shown in (3)

$$P = E - \frac{1}{g}\int_{p_b}^{p_t} \frac{\partial q}{\partial t}\, dp - \frac{1}{g}\int_{p_b}^{p_t} \nabla \cdot q\mathbf{V} dp - \frac{1}{g}\int_{p_b}^{p_t} \frac{\partial q\omega}{\partial p}\, dp. \tag{3}$$

Eq. (3) is the equation for conservation of water in a vertical column. The P and E are precipitation and evaporation. The integration limits p_b and p_t refer to pressure at the bottom and top of a layer. Other symbols have their usual meteorological meanings. In (3), moisture storage and the transport of liquid and frozen water in the layer are assumed to be negligible for large scale systems (Palmen and Newton, 1969). The second term on the right is the local change of specific humidity in the column. This term was computed over the days which were followed by a subsequent set of observations. It proved to be at least one order of magnitude smaller than the other terms of the equation and thus was neglected in the final budget computations. The third term on the right represents the horizontal trans-

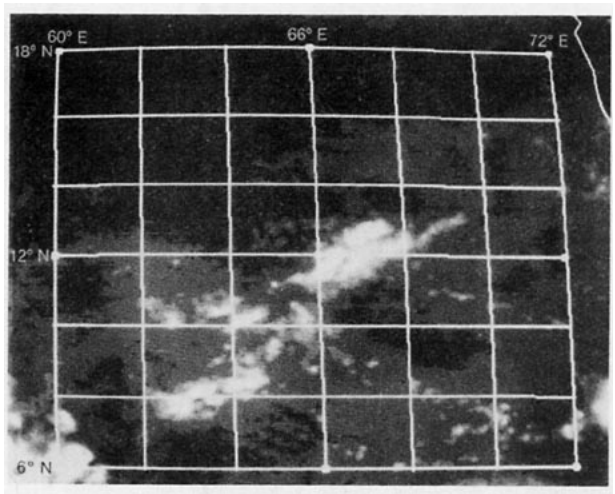

FIG. 2. Infrared image for 0800 GMT 29 May 1979. The coastline of India can be seen in the upper right corner. Gridding is 2°.

port of moisture. It was separated into a moisture advection and a moisture convergence term. The last term represents the vertical transport of moisture. The integral is zero due to the assumptions imposed on the vertical velocity at the bottom and top of the volume. This term was, however, evaluated at individual levels and was consistently one or two orders of magnitude less than the other terms. The 1° gridding is probably not sufficiently dense to observe the mesoscale cumulus contribution that would cause this term to be large. After discarding the local change term and the vertical transport term and having made the mentioned changes, (3) becomes (4) and is the basis for the moisture budget computations.

$$P = E - \frac{1}{g}\int_{p_t}^{p_b} q(\nabla \cdot \mathbf{V})dp - \frac{1}{g}\int_{p_t}^{p_b} (\mathbf{V} \cdot \nabla q)dp. \quad (4)$$

Evaporation of falling rain is assumed to be negligible in the subcloud layer over a tropical ocean and is not included in (4). Surface evaporation is estimated using the bulk aerodynamic method as discussed by Rao *et al.* (1981). The equation for evaporation is

$$E = C_d \rho_a (q_s - q_a) V, \quad (5)$$

where C_d is a drag coefficient, ρ_a is the sea level air density and $(q_s - q_a)$ is the difference between saturation specific humidity at sea level and the actual specific humidity at ship deck level. The V is wind speed at ship deck level. As suggested by Rao *et al.* (1981), the drag coefficient was given two wind speed dependent values. For $V < 13$ m s^{-1}, C_d is 1.4×10^{-3} and for $V \geq 13$ m s^{-1}, C_d is 1.6×10^{-3}.

Before (4) could be integrated from 1000 to 100 mb, winds needed to be generated at 1000 mb and above 350 mb. Although dropsondes reported temperature and humidity below or near 1000 mb, they typically did not report winds lower than 950 mb and were released below 300 mb. The surface ship observations were not dense enough to provide an estimate of the 1000 mb winds, especially in the disturbed areas. Satellite-derived winds as described earlier were used to represent the 200 mb level. Eq. (6) (Hess, 1959) was used to generate winds for the 1000 mb level,

$$U_{1000} = \frac{U_{950}}{(Z_{950}/Z_{1000})^m}. \quad (6)$$

This equation has been empirically fit with m for various thermal lapse rates. Over the Arabian sea, $m \approx 0.12$. Using available soundings from ships, it was found that the ratio of the heights, Z_{950}/Z_{1000}, averaged 8 for premonsoon and 10 for active monsoon. As an approximation this yields

$$U_{1000} = U_{950} \times 0.75. \quad (7)$$

This provided estimated winds for the 1000 mb surface. Veering of the wind in this layer over the ocean was generally less than 10 deg and since this was also variable, no veering correction was applied. Wylie and Hinton (1981) comparing low-level satellite-derived winds to ship reports have found a relationship very similar to (7) for winds over the Indian Ocean during the month of June, 1979.

With the necessary data generated, (4) was integrated from 1000 to 350 mb in 50 mb layers. The last two layers were integrated from 350 to 200 mb and from 200 to 100 mb. The 200 mb level values of specific humidity were taken from mean ship and island radiosondes for that day. Specific humidity was assumed to be zero above 200 mb. Because specific humidity was very small above 350 mb, the budget results were affected little by the results of the upper two layers. The actual height of the 1000 mb surface varied from −50 m to 110 m over the study days, but for most of the domain, the 1000 mb surface is within a few tens of meters of the actual surface. The errors resulting in

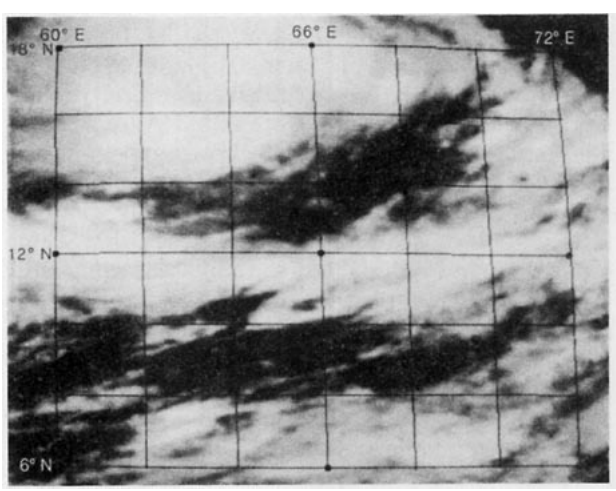

FIG. 3. As in Fig. 2 but for 0800 GMT 17 June 1979.

approximating the surface as 1000 mb are small and at worst may amount to 2 to 5% of the budget totals.

4. Results

Before discussing the results of the moisture budget computations, it is useful to take a brief look at the convective activity present before and after the 1979 monsoon onset. Fig. 2 is an infrared image from GOES-Indian Ocean which displays the budget area at 0800 GMT 29 May 1979. No deep convective activity is present in the budget area (clouds seen near the center of the image are middle-level and cirrus clouds). This was typical of premonsoon days. There was a disturbance to the southwest of the budget area. In contrast, Fig. 3 is a similar image at 0800 GMT 17 June 1979. A tremendous increase in convective activity has oc-

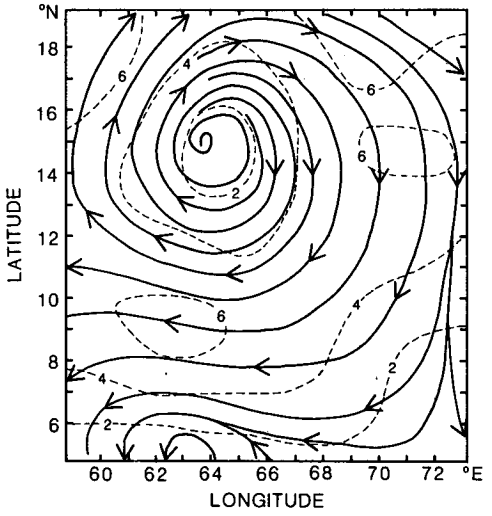

FIG. 4. Streamlines and Isotachs of the 900 mb wind field on 29 May 1979. Isotachs are contoured at 2 m s^{-1}.

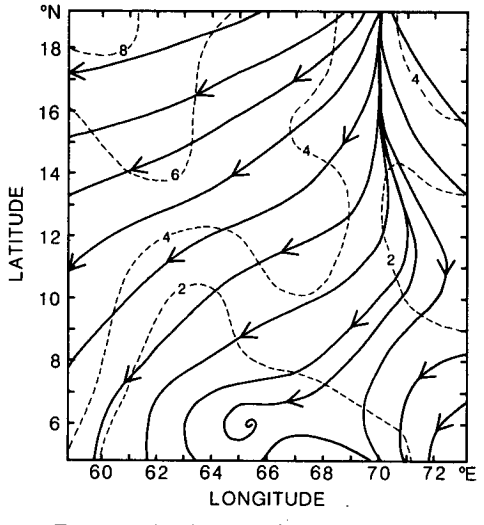

FIG. 5. As in Fig. 4 but for 3 June 1979.

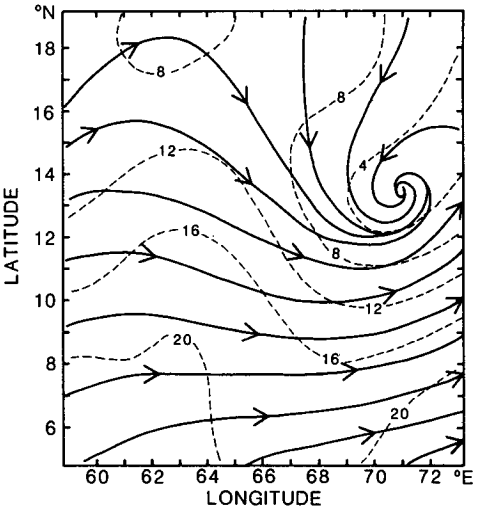

FIG. 6. As in Fig. 4 but on 15 June 1979. Isotachs are contoured at 4 m s^{-1}.

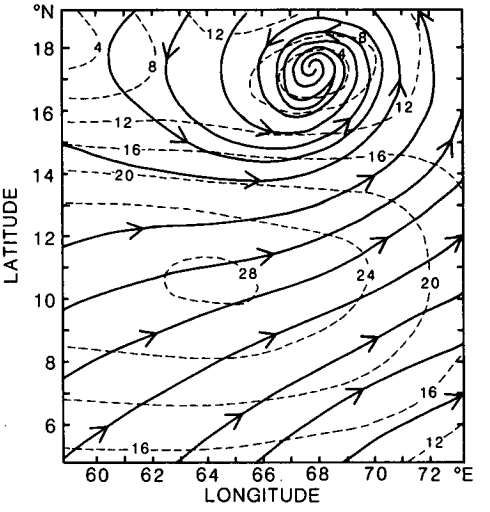

FIG. 7. As in Fig. 6 but for 17 June 1979.

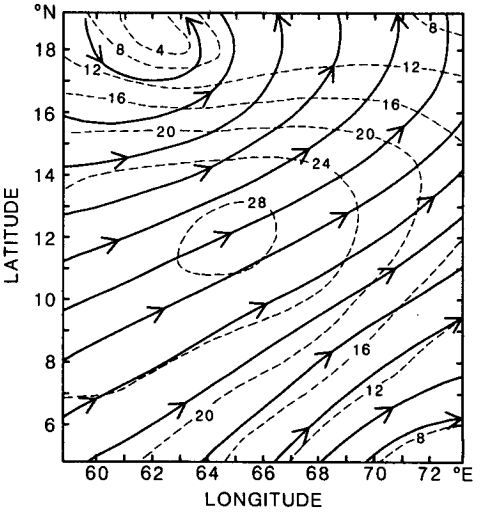

FIG. 8. As in Fig. 6 but for 18 June 1979.

curred. The upper left portion shows the location of the monsoon onset vortex, which intensified at about 14°N, 71°E on 15 June and travelled northwest towards Arabia to reach the position shown in Fig. 3. On 17 June, an intense band of convection is located at about 12°N. The axis of the Somali jet is shown by a cleared region south of 8°N. Although not evident in this image, the activity south of 8°N is decaying rapidly. This will be discussed later. The contrast between the two images is striking.

a. Kinematic fields

Diagrams of streamlines and isotachs are presented in Figs. 4–8 for the 900 mb level of each day during the budget study in order to give the reader background on the nature of the low-level flow on individual days. As can be seen in Fig. 4, the Arabian Sea was dominated by a strong anticyclone on 29 May. This gave way to a difluent ridge on 3 June as shown in Fig. 5. The onset vortex and location of the low-level southwesterly jet can be seen in Figs. 6 to 8 from 15, 17, and 18 June 1979. The level of maximum wind speed was found to be at 850 mb on the three onset period days. The westerlies were quite deep and extended to 400 mb on these days. The maximum strength of the low-level jet was about 32 m s^{-1} at 850 mb on 18 June. The location of this maximum was virtually at the center of the budget area.

Just as the satellite imagery in Figs. 2 and 3 show a remarkable change from premonsoon to monsoon onset, the kinematic fields of divergence and vertical velocity show a marked reversal. This is to be expected viewing the differences between the wind fields of Figs. 4 and 5 to those of the onset period shown in Figs. 6 to 8.

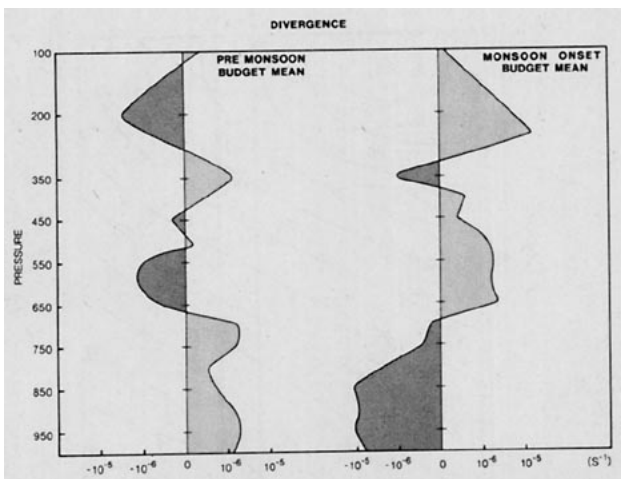

FIG. 9. Mean divergence profiles for premonsoon and monsoon onset. Profiles shown are averages for the 12° square budget area. Negative values represent convergence. The "0" reference point is used for levels which have absolute values less than 1×10^{-7} s^{-1}.

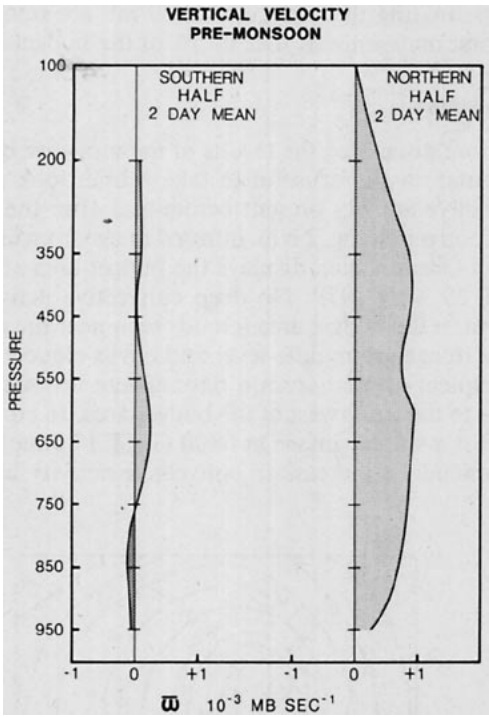

FIG. 10. Profiles of premonsoon average vertical velocity. Southern half refers to half of the budget area south of 12°N. The same convention applies to northern half. Data are two-day means.

The mean divergence profile is shown in Fig. 9 for the two premonsoon days and the three monsoon onset days. The premonsoon period was marked by divergence below 700 mb. Two levels of convergence were present in the mid- to upper troposphere. The onset period shows nearly a mirror image reversal of this pattern and as illustrated in Fig. 9, divergence is an order of magnitude greater. Strong low-level convergence and two levels of outflow exist. This suggests the contribution of cumulus congestus as well as deep convection in the generation of divergence aloft. This outflow pattern is also seen for individual quadrants (6° × 6° areas) within the budget area. The multiple outflow levels are similar to findings of Thompson *et al.* (1979) for the GATE region of the tropical eastern Atlantic. The midtropospheric convergence which is shown weakly at 350 mb, is stronger on individual days, but at slightly different levels.

Vertical velocity profiles for premonsoon and monsoon onset are shown in Figs. 10 and 11. The budget area was divided into a northern and southern half for illustration of north to south differences. During premonsoon, the northern half of the budget area is dominated by subsidence. The southern half, however, shows little mean vertical motion. There, the influence of a loosely defined ITCZ and associated disturbances south of 6°N had begun to affect the vertical velocity profiles. During the onset period, strongest mean upward motion is found north of 12°N. As expected

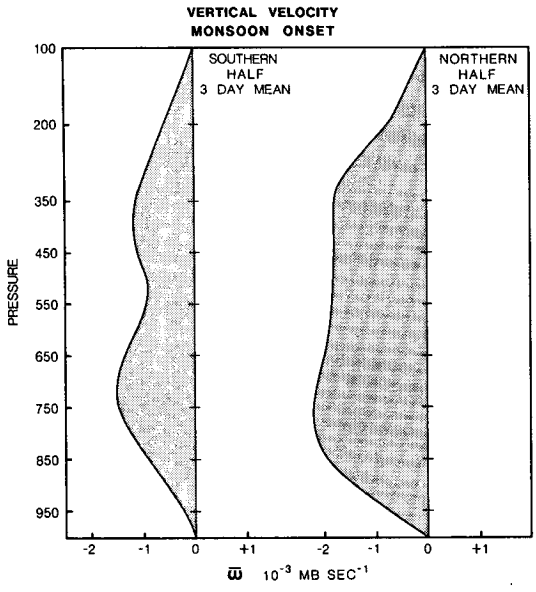

FIG. 11. As in Fig. 10, but for the monsoon onset period. The data are 3-day means.

from the mean divergence profiles, a double maximum in the vertical velocity can be seen near 700 and 350 mb in Fig. 11. The southern half of the budget area is highly disturbed on 15 June. This provides the majority of the upward motion for the southern half of the budget area seen in Fig. 11.

Zonally averaged vertical velocity for the 3-day monsoon onset period is shown in Fig. 12. Clearly seen is a distinct northern shift of the principal cell of convection from 15 June (Fig. 12a) to 18 June (Fig. 12c). On the 15th, the low-level jet was located on a nearly east–west axis just north of 6°N. Two cells of maximum upward motion were north and aloft of the low-level jet. Upward motion was dominant throughout the budget area. The vertical velocity cell due to formation of the onset vortex can be seen at 15°N at 750 mb. It is interesting to see that this cell did not yet have a corresponding maximum aloft. This suggests that the vortex was not fully developed and that deep convection was not as widespread as on the following two onset period days. On 17 June (Fig. 12b) the low-level jet had shifted north to a position about 10°N and a corresponding shift in the vertical velocity field can be seen. The convergence north of the low-level jet and that of the onset vortex had combined to form a large double maximum cell of vertical motion. To the south of the jet, subsidence appeared in the budget area. This had a stabilizing and drying effect at mid-levels. The band of cloudiness seen in Fig. 2 at 7°N disappeared within hours. Finally, on 18 June (as the southwest low-level jet displaced further north to 12°N.), the budget area was divided into two distinct regions, active convection north of 12°N and subsidence and drying south of 12°N. The moisture budget was greatly influenced by these features during the monsoon onset.

Figure 13 depicts the premonsoon and onset period average profiles of specific humidity for the budget area. Daily mean specific humidity profiles are shown in Fig. 14. A tremendous moistening occurs between 29 May and 17 June. The midtroposphere shows as much as a 5 g kg^{-1} increase in moisture between premonsoon and monsoon onset. The 18th shows a drying from the moisture peak of 17 June. This drying is apparently due to fallen precipitation, and in part due to subsidence (seen in Fig. 12), and advection of drier air from the west (as will be seen later).

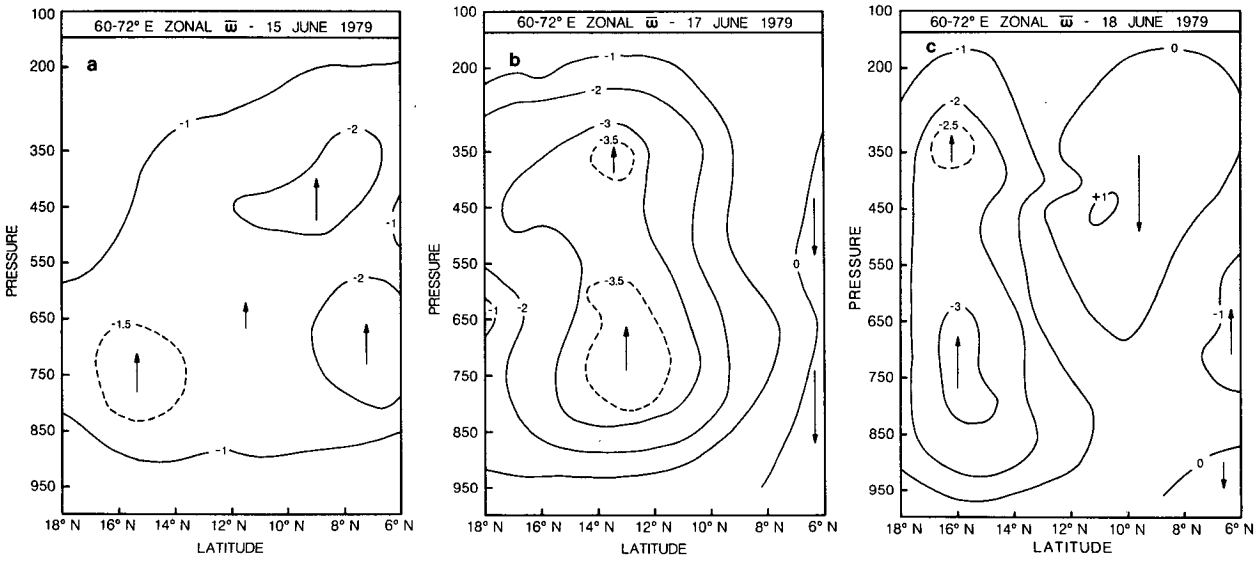

FIG. 12. Zonally averaged vertical velocity is plotted against pressure for (a) 15 June, (b) 17 June and (c) 18 June. Arrows indicate the direction of motion. Contouring is in 10^{-3} mb s^{-1}.

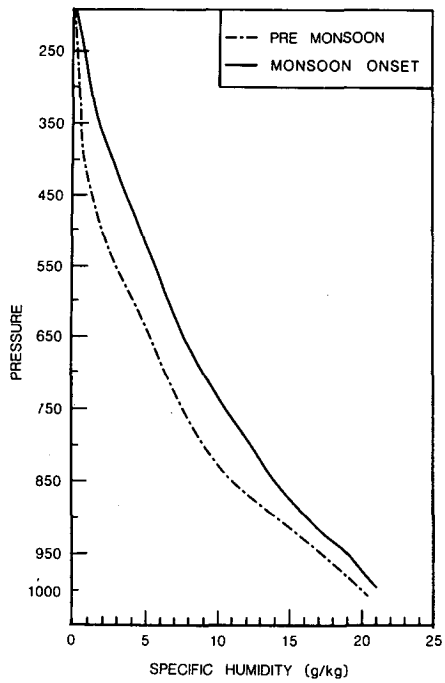

FIG. 13. Specific humidity plotted against pressure for premonsoon and the monsoon onset period. The profiles are means over the entire budget area.

b. Moisture budget results

General features of the moisture budget computed from (4) are shown in Fig. 15. The means of the premonsoon budget terms are shown in Fig. 15a and the monsoon onset budget means are shown in Fig. 15b. Moisture advection had a net drying effect during monsoon onset and a net moistening effect during premonsoon (Fig. 15d). Moisture convergence is clearly the dominant term of the budget equation and the maximum moisture convergence was on 17 June. Net moisture divergence occurs on both premonsoon days (Fig. 15c). Monsoon onset average precipitation [calculated as a residual of (4), Fig. 15b] was slightly over 1 mm h^{-1} over the budget area of 1.7×10^6 km^2.

Daily evaporation computed for four quadrants of the budget area, each a 6° × 6° square, is shown in Table 1. Although the difference between sea level saturation and deck level specific humidity decreased with increasing convective activity, the intensification of the low-level jet caused evaporation to be three times higher during onset than during the premonsoon period. Evaporation was strongest south of 12°N and west of 66°E where it averaged 16 mm day^{-1}. Rao *et al.* (1981) shows an average evaporation over the Arabian Sea of 4–6 mm day^{-1} for June 1963. The smaller area of this budget volume and its location relative to the low-level jet, account for the higher values of evaporation found in this study.

Although the moisture advection term in (4) is about 3 times smaller than the convergence term, some interesting results are found in looking at the advection term on individual days. Moisture advection is shown in Figs. 16 and 17 for 3 and 17 June. Each day is representative of its period. On 3 June, positive moisture advection is present above 800 mb. The negative (dry air) advection below 800 mb is the result of continental air flowing to the southwest from India. The exception noted below 800 mb for the NW quadrant is because this quadrant had previously been very dry and the NE flow has picked up enough moisture at low levels to have a moistening effect for this quadrant. Almost all of the region displaying positive moisture advection above 800 mb has a southerly component to the wind. The southern border of the budget area lies north of a band of deep convection which is the apparent source of this moistening. Advection had a net moistening role in the midtroposphere during premonsoon.

In contrast to the premonsoon days, the advection of dry air from the west dominates the southern two quadrants of the budget area on 17 June. Positive moisture advection is still seen at low levels in the northern half of the budget area. There is considerably drier air to the south and west of the budget area on this day especially above 900 mb. South of 12°N, a rapid decrease in convective activity occurred at the time of this influx of relatively drier air from the west. The source of this dry air is not immediately obvious but it appears that the airflow from the southern hemisphere at these levels is relatively drier than the local air over the southern budget area. Ghosh *et al.* (1978)

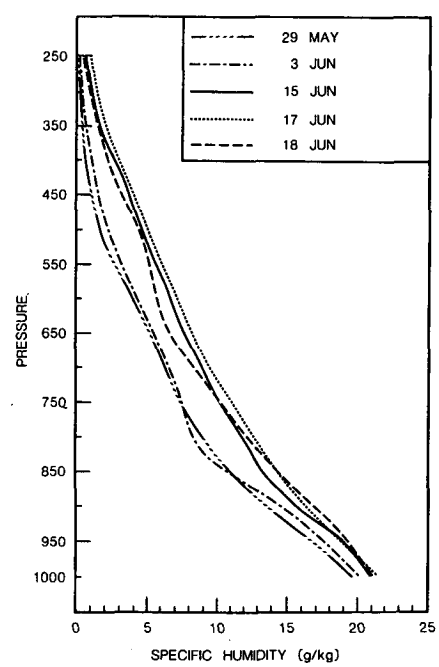

FIG. 14. As in Fig. 13 but profiles are for individual budget days.

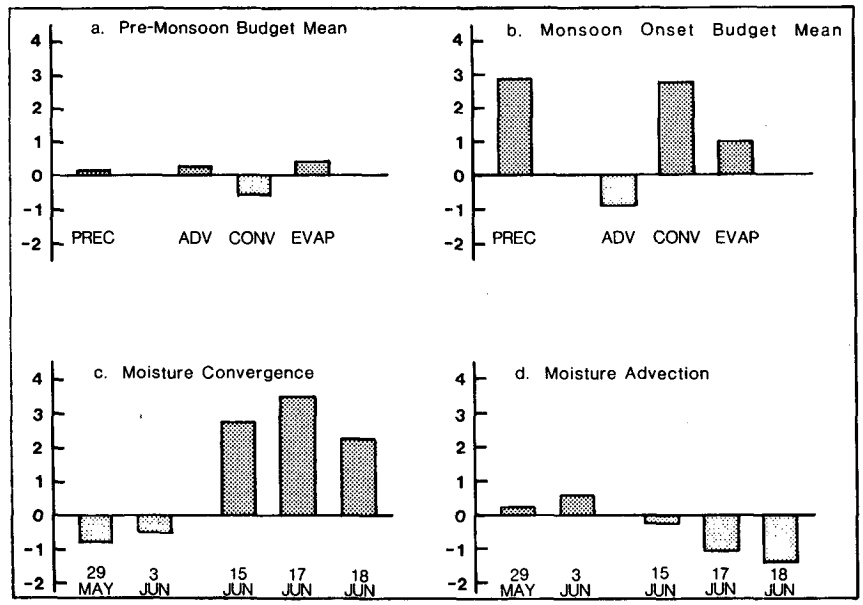

FIG. 15. Moisture budget calculation results are shown for (a) premonsoon, (b) monsoon onset, (c) daily mean moisture convergence and (d) daily mean moisture advection. Positive values indicate a net gain to the budget volume. Precipitation resulting as a residual of the budget equation is plotted in (a) and (b). Shown as a positive value, it is the amount which must fall out of the budget volume in order to balance the budget terms. Units are 10^{-4} kg m^{-2} s^{-1}.

have shown that during periods of strong monsoon circulation, precipitable water is considerably lower (by as much as 50%) over the equatorial region than over the domain of our moisture budget. This agrees with the advection of dry air on 17 June. The subsidence seen aloft and south of the low-level jet also accounts for some of the drying out of the southern portion of the budget area. Satellite infrared imagery of the 15 and 18 June are shown in Figs. 18 and 19. The drying of the southern half of the budget volume can be seen clearly by comparing the sequence of Fig. 18, 3, and 19.

Zonal and meridional profiles of moisture advection are shown in Fig. 20 for the monsoon onset period. The values are averages through the entire volume (1000 mb to 100 mb). These profiles show drying starting in the southwest, which gradually moves east and north through the budget area. The drying was strongest south of 12°N. A second pulse of dry air enters the western edge of the budget volume on the 18th between 11 and 14°N. This was the result of dry continental air drawn off Arabia by the northwest circulation around the onset vortex.

While moisture advection was having a drying effect on 17 and 18 June, horizontal moisture convergence continued to be positive through the monsoon onset period. That is to say, that even though drier air was entering portions of the budget area, moisture within the budget area continued to be processed into precipitation primarily due to strong net low-level convergence. The dominance of moisture convergence seen in Fig. 15 has been shown for other cases by Carr and Bosart (1978) and Hudson (1971). Fig. 21 shows the premonsoon and monsoon onset means of moisture convergence. As expected, moisture convergence was dominant at low-levels during the onset period.

TABLE 1. Evaporation in units of 10^{13} kg day^{-1} for the budget area. Quad refers to a 6° × 6° or 6° × 12° portion of the budget area as located by directional position. (North and South are 6° × 12° halfs of the budget area).

QUAD	29 May	3 June	Pre-monsoon	15 June	17 June	18 June	Monsoon onset
NW	0.08	0.16	0.12	0.13	0.15	0.59	0.29
NE	0.19	0.15	0.18	0.16	0.13	0.34	0.21
SW	0.08	0.11	0.10	0.32	0.54	0.66	0.51
SE	0.07	0.19	0.13	0.32	0.45	0.38	0.38
North	0.27	0.31	0.30	0.29	0.28	0.93	0.50
South	0.15	0.30	0.23	0.64	0.99	1.04	0.89
Budget total	0.42	0.61	0.53	0.93	1.27	1.97	1.39

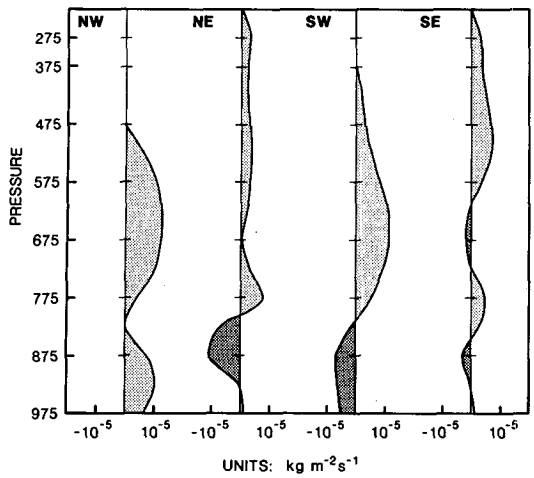

FIG. 16. Moisture advection for 3 June 1979. Moistening is shown by positive values. Each profile represents a 6° × 6° quadrant of the budget volume and is labeled by directional position.

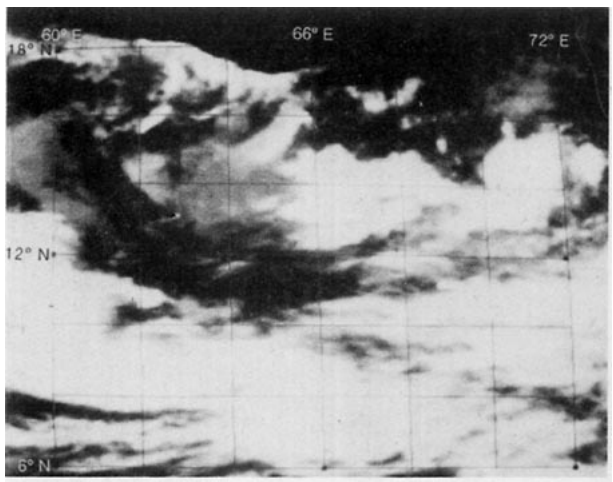

FIG. 18. Infrared image from GOES-IO for 0730 GMT 15 June 1979. Formation of the onset vortex is at 13°E, 71°E. Gridding is 2°.

This agrees with the findings of Ghosh *et al.* (1978) who found that the region between 60 and 70°E was a region of net moisture convergence during the 1973 monsoon season. Two levels of moisture outflow appear on the onset days. The weakness of the upper-level outflow was due to the decrease in specific humidity with height, not the intensity of the divergence at upper-levels. The profile for premonsoon is almost the opposite of that for monsoon onset. This is to be expected from the similar findings for divergence and vertical velocities.

c. *Precipitation fields*

Precipitation estimated at grid points as a residual of (4) is shown for 15 and 18 June in Figs. 22 and 23. The validity of the budget computations is supported not only in the area average values displayed to this point, but also in the detailed reflection of convective features seen in the satellite images of Figs. 18 and 19. To serve as a reference, the location of the low-level jet axis is depicted as a dashed straight line on the precipitation maps. On all three monsoon onset days, the heaviest precipitation is north of the jet. To the south, the influence of subsidence and the advection of drier air can be seen in Fig. 23 and in satellite images (Figs. 3 and 19). The development of the onset vortex can be seen in both satellite imagery and in the budget precipitation maps. The convective cloud cover seen in the NE quadrant of Fig. 18 increased dramatically over the next six hours. This is apparently captured in the precipitation map (Fig. 22) by the widespread precipitation maximum in the NE quadrant. The locations of precipitation bands on 15 and 18 June also agree very well with the convective bands seen in the satellite imagery. The separation of the onset vortex

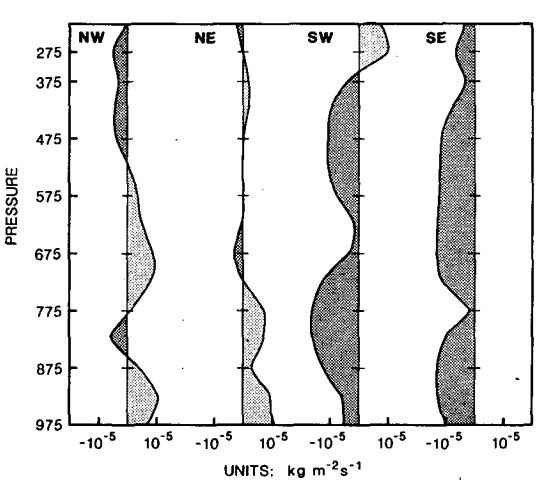

FIG. 17. As in Fig. 16 but for 17 June 1979.

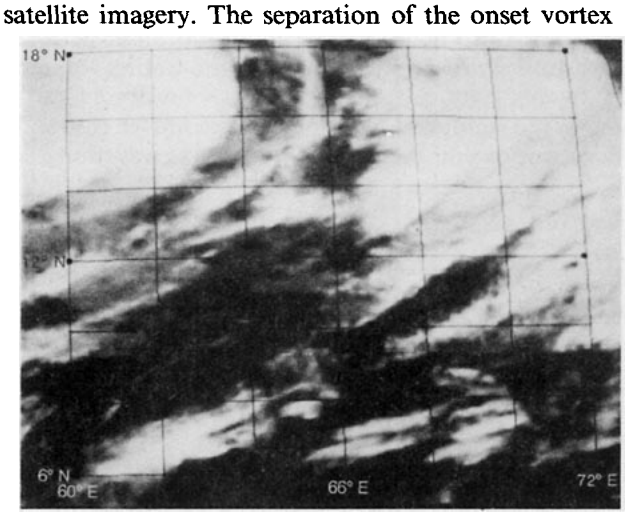

FIG. 19. As in Fig. 18 but for 0800 GMT 18 June 1979.

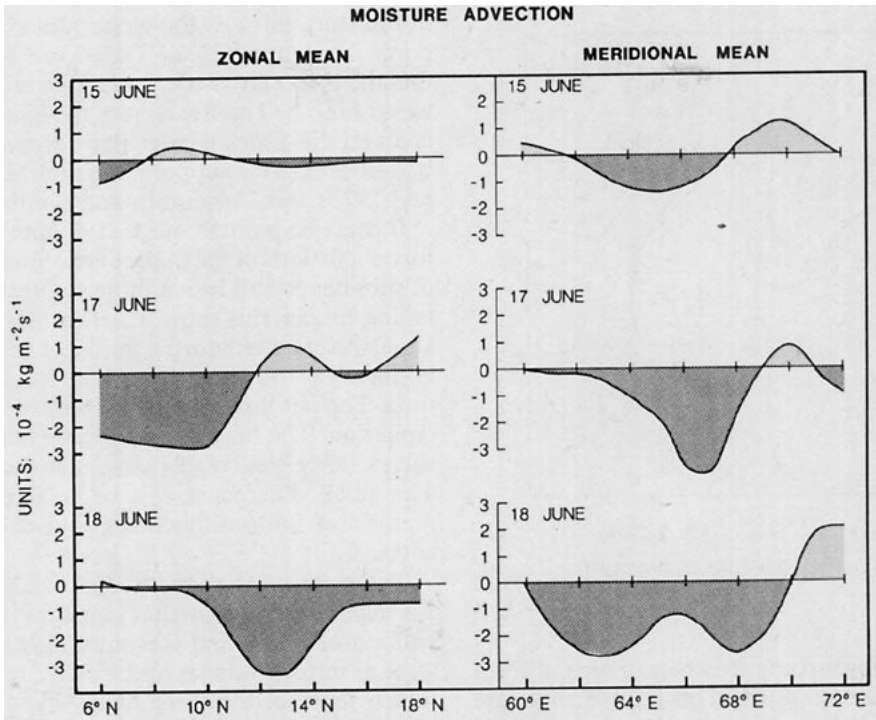

FIG. 20. Zonal and meridional average profiles of moisture advection. Negative values represent drying.

and the convergence off India's west coastline are captured in Fig. 23. The small squall type disturbances south of 12°N are also suggested in the budget results. Precipitation maps for the other days show similar agreement.

5. Discussion

Direct comparison of this study to those previously done for the Arabian Sea is not possible due to the difference in location of the various budget volumes. The relative short time span of this study may be more applicable to the onset of this monsoon season than to long-term climatological averages as computed by others. However, in order to make possible some com-

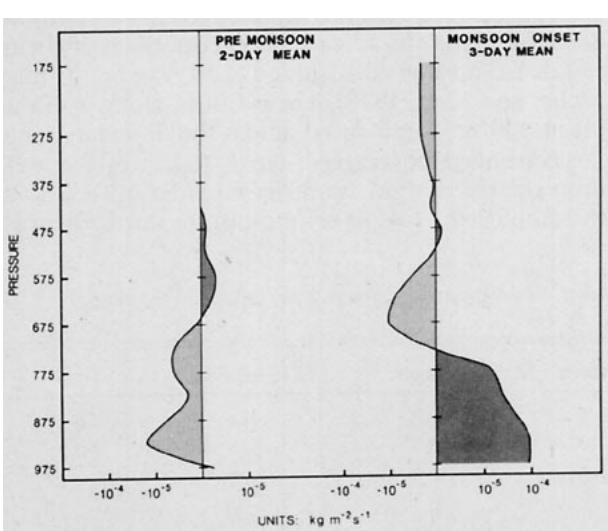

FIG. 21. Moisture convergence average profiles for premonsoon and monsoon onset. Positive values are moisture convergence.

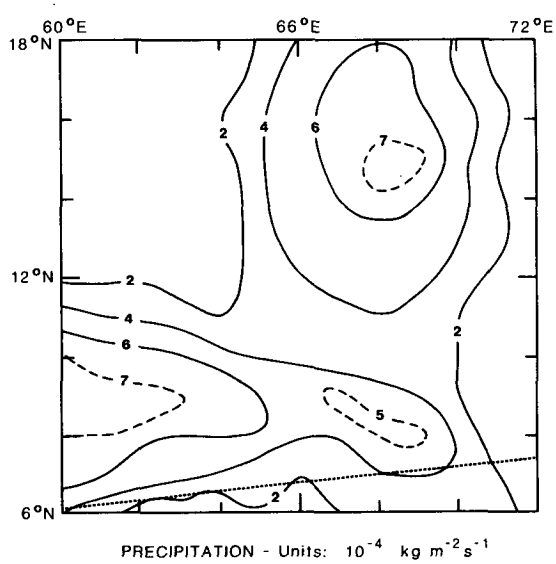

FIG. 22. Precipitation field for 15 June 1979 computed as a residual of the moisture budget. Contours are at 2×10^{-4} kg m^{-2} s^{-1} (supplemental contours are dashed). The dotted straight line indicates the axis of the low-level wind jet at the 850 mb level. Note: 2.78×10^{-4} kg m^{-2} s$^{-1} \approx 1.0$ mm h^{-1}.

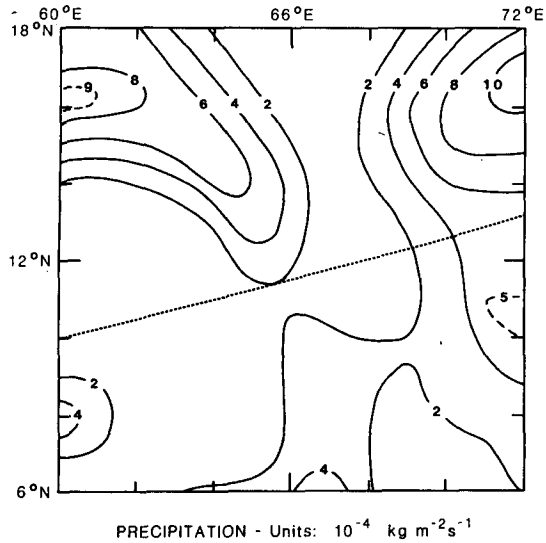

FIG. 23. As in Fig. 22 but for 18 June 1979.

parisons of this budget study to others, a second form of the budget was computed. The flux of moisture across a budget wall is given as

$$\text{Flux} = \frac{1}{g}\int_{p_t}^{p_b}\int_0^L \bar{V}_n\bar{q}dLdp. \qquad (8)$$

In (8) $\bar{q}$ is the average specific humidity for the layer and $\bar{V}_n$ the average component of the wind perpendicular to the boundary wall and L the length of the boundary wall. As before, p stands for pressure. The result is the average flux of moisture across a boundary wall in the pressure layer p_b to p_t. The net flux into the budget volume is the horizontal flux of (8) plus evaporation from the Arabian Sea [computed as previously mentioned using (5)]. Table 2 contains the flux of moisture across budget boundaries computed from (8) and evaporation from the Arabian Sea surface. During premonsoon, outflow is strongest along the western boundary. This is due to dominant northeasterly low-level flow. Evaporation exceeds inflow along the southern boundary (inflow was above 800 mb).

With the development of a strong southwesterly low-level jet, the onset period days show the greatest influx of moisture through the western boundary. This supports the contention of Cadet and Reverdin (1981) that the major cross-equatorial flux of moisture occurs west of 60°E. The flux across the southern boundary is about 1.7 times greater than evaporation over the budget area. This supports the findings of Saha (1970 and 1973) and Hastenrath and Lamb (1980).

It must be pointed out that despite these boundary fluxes, portions of the budget areas under the influence of subsidence and losing more moisture than they are taking in can still show a net drying (as seen on 18 June). As expected during the onset period, the eastern boundary is the principal sink of moisture for the volume. The net flux into the volume is available as precipitation. The magnitude of these flux computations agrees fairly well with the results shown in Fig. 15. The small differences can be accounted for by the method of finite differencing and calculation differences.

The magnitude of the budget flux shown in Table 2 is slightly higher than that found for the larger budget volume of Cadet and Reverdin (1981). Their values were monthly averages and would not be expected to match those of the three highly disturbed days used here. The general agreement lies in the direction of the flux and by being in the same order of magnitude.

The values shown in Table 2 and Fig. 15 do not include loss to the volume through the outflow of ice in the form of cirrus. At first glance at the satellite images of Figs. 18, 3 and 19 this might seem to be a significant source of error. To evaluate the magnitude of this loss, average coverage of cirrus cloud was computed using the McIDAS (Man-computer Interactive Data Access System) of the University of Wisconsin-Madison. This was done by thresholding infrared brightness into two apparent cirrus thicknesses. Brightness values of 160 and 180 digital counts were used. Thin cirrus was estimated to have a 1 km depth and dense anvil cirrus was assumed to have an outflow depth of 3 km. The average water equivalent of cirrus clouds has a value of 0.1 to 0.4 $\times$ 10^{-3} kg m^{-3} (Pruppacher and Klett, 1978). These values, along with the mean 200 mb wind speed across the boundary, and the percentage coverage of cirrus (taken in the area immediately upwind from the boundary) were used to compute the loss of solid moisture through cirrus

TABLE 2. Water vapor flux across boundaries of the budget volume. Positive values represent a net influx to the volume. Units are in 10^{13} kg day^{-1}.

Date	Western	Eastern	Northern	Southern	Evaporation	Total
29 May	−1.3	0.0	+0.2	+0.5	+0.4	−0.2
3 June	−2.5	+1.3	+1.0	+0.1	+0.6	+0.5
Premonsoon	−1.9	+0.6	+0.6	+0.3	+0.5	+0.1
15 June	+4.6	−2.9	+1.7	+1.3	+0.9	+5.6
17 June	+7.3	−7.9	+0.9	+2.7	+1.3	+4.3
18 June	+8.9	−6.7	−3.1	+2.9	+2.0	+4.0
Active monsoon	+6.9	−5.8	−0.2	+2.3	+1.4	+4.6

outflow. The predominant 200 mb flow is easterly so the greatest cirrus outflow occurs across in the western boundary and there is a net inflow along the eastern boundary.

Using the most extreme measurements over the three-day monsoon onset period, and varying the water content from 0.1 to 0.4 ($\times 10^{-3}$) kg m^{-3}, the loss through cirrus outflow ranges from 3×10^{11} to 1.2×10^{12} kg on 17 June. June 15 showed a loss of about 2×10^{11} kg and the 18th showed a net gain equalling the loss of the 15th. While these numbers are large amounts of water, they account for about 1–3% of the total budget flux as seen in Table 2. The loss through cirrus outflow appears to be negligible.

In a final evaluation of the budget results, it would be ideal to have ground observations of precipitation to test the overall accuracy of the computations. Due to location, this is not possible. In an effort to evaluate the budget validity, two independent estimates of precipitation on the monsoon onset days were made. The first is a parameterization using the gridded data. The second is a satellite precipitation estimating scheme.

Krishnamurti *et al.* (1980) summarize several cumulus parameterization schemes. Of these, they find that a term shown as (9) (a part of Kuo's (1974) parameterization technique) had one of the best relationships to observed rainfall during GATE.

$$R = -\frac{1}{g}\int_{p_t}^{p_b} \bar{\omega}\frac{\partial q}{\partial p}\,dp. \tag{9}$$

In (9), R is rainfall and $\bar{\omega}$ the mean vertical velocity in the layer. The term $\partial q/\partial p$ can be thought of as the lapse rate of specific humidity. This equation was evaluated and results are shown in Fig. 24 by budget area $6° \times 6°$ quadrant daily mean. Only in the cases where moisture advection and/or evaporation were large, did this value differ much from the budget computations. Its tendency was to underestimate.

In a second independent estimate, satellite images from 0730 and 0800 GMT were used with the Stout, *et al.* (1979) life history technique for estimating precipitation. Rainfall is given as a function of the area covered by deep convective clouds. The relationship is shown in

$$R = a_0 A + a_1 dA/dt. \tag{10}$$

Here R is the volumetric rainfall from convective clouds and A is the area covered by clouds of a prescribed brightness threshold. The coefficients a_0 and a_1 are determined for the GATE area and are used here for this comparison estimate. Since both regions are over tropical ocean of about the same latitude, the GATE derived relationship should provide a useful comparison. The average of visible and infrared estimates is depicted on Fig. 24. The satellite technique estimated about 15% lower values of precipitation than did the moisture budget. Most of this difference occurred in the northeast quadrant on 15 June. The budget apparently captured the rapid growth of the onset vortex. In contrast, the satellite images at 0730 and 0800 GMT do not show the rapid growth of the precipitation area of the onset vortex that occurred over the next 6 to 12 hours. The satellite estimating technique may not have yielded a high enough volumetric rain rate for this deep convection. The budget computed precipitation does agree remarkably well with these two independent estimates.

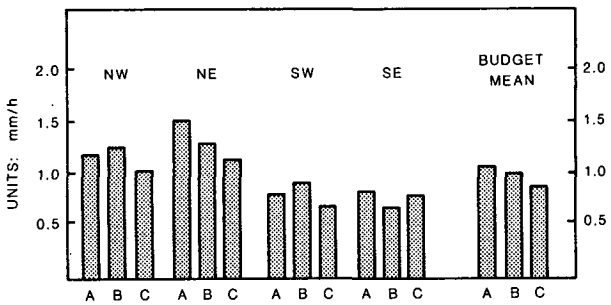

FIG. 24. Monsoon onset precipitation estimates. Values represent a 3-day mean. Each quadrant is labeled by its directional position and the value represents an average over the $6° \times 6°$ square. The estimates are labeled as follows: A, Moisture budget; B, Krishnamurti parameterization; C, Satellite technique—Stout, Martin, and Sikdar. Budget mean refers to the 3-day average over the entire budget area.

6. Conclusions

Detailed moisture budgets have been presented for the northeastern Arabian Sea based on data from ships, aircraft dropsondes, ship, island, and coastal radiosonde, and satellite-derived 200 mb winds. Two days' data representing premonsoon and three days' data representing the monsoon onset have been used to compute the moisture budgets. There was a remarkable change from conditions of premonsoon to those during the three monsoon-onset days. Specific humidity in the middle troposphere increased as much as 5 g kg^{-1} from premonsoon to monsoon onset. This was a result of deep convection during monsoon onset and at least partially due to advection of moisture from the south of the budget area at levels above 800 mb during premonsoon. The kinematic profiles of wind, divergence, and vertical velocity undergo almost a complete reversal from conditions seen during premonsoon. Evaporation increased with the strengthening of the low-level jet and reached a maximum in the southern half of the budget area (3 to 4 times greater than that estimated during premonsoon).

The moisture budgets also depicted the convective features seen in satellite imagery well. Maximum vertical velocity was calculated where disturbed regions were viewed by the satellite. The formation and the movement of the onset vortex and the low-level jet were also depicted by the budget precipitation maps. The drying of the southern half of the budget area, visible in the satellite images of 17 and 18 June, was the result of the advection of relatively drier air from

the west and subsidence aloft and to the south of the low-level jet.

Comparisons of these budgets to previous work done over the Arabian Sea support the importance of cross-equatorial moisture flux (especially west of 60°E). The flux of water vapor across the budget boundaries agrees in magnitude with previous estimates. However, as seen on 17 June, the cross-equatorial flux does not always result in a moistening of the Arabian sea air-mass. The inclusion of an estimate of the loss of moisture due to cirrus outflow showed the loss to be about 1–3% of the total budget flux. It was the low-level horizontal moisture convergence that dominated the budget computations.

Two independent estimates were made of precipitation over the budget area on the three monsoon onset days. The good agreement of these estimates with the values computed from the moisture budgets, provides evidence of the validity of the combined data base and of the moisture budget results.

The data generated by these moisture budgets have provided interesting insight into the relationship between the low-level jet and convection over the Arabian Sea. This relationship and the possible link between the low-level jet and the onset vortex are areas which need further research. As a possible extension of this work, we hope to study 3 days of observations near 24 June 1979 to see what differences occur after a mature active monsoon is established and the onset vortex has dissipated.

Acknowledgments. Grateful thanks are due Drs. Robert Ballentine and Hsiao-ming Hsu and David Miller of the University of Wisconsin-Milwaukee and Dr. David W. Martin of the Space Science and Engineering Center, University of Wisconsin-Madison for their advice and comments offered throughout the period of research and writing of this paper. We are indebted to Drs. Donald Wylie and John Young of the University of Wisconsin-Madison for help in obtaining some of the data needed for this work. This research was supported by the National Science Foundation (GARP Office) under Grant ATM-7920850. Publication charges were supported by NSF Grant ATM-80-20895.

REFERENCES

Barnes, S. L., 1964: A technique for maximizing details in numerical weather map analysis. *J. Appl. Meteor.*, **3**, 396–409.

Cadet, D., 1981: Water vapour transport over the Indian Ocean during summer 1975. *Tellus*, **33**, 476–487.

——, and M. Desbois, 1980: The burst of the 1978 Indian Summer Monsoon as seen from METEOSAT. *Mon. Wea. Rev.*, **108**, 1697–1701.

——, and G. Reverdin, 1981: The monsoon over the Indian Ocean during summer 1975. Part I: Mean fields. *Mon. Wea. Rev.*, **109**, 148–158.

Carr, F. H., and L. F. Bosart, 1978: A diagnostic evaluation of rainfall predictability for Tropical Storm Agnes, June 1972. *Mon. Wea. Rev.*, **106**, 363–374.

Fankhauser, J. C., 1969: Convective processes resolved in a mesoscale rawinsonde network. *J. Appl. Meteor.*, **8**, 778–798.

Fein, J. S., and J. P. Kuettner, 1980: Report on the summer MONEX field phase. *Bull. Amer. Meteor. Soc.*, **61**, 461–474.

Findlater, J., 1969: A major low-level air current near the Indian Ocean during the northern summer. *Quart. J. Roy. Meteor. Soc.*, **95**, 362–380.

——, 1971: Mean monthly air flow at low levels over the Western Indian Ocean. *Geophys. Mem.*, **115**, HMSO, London, 53 pp.

Ghosh, S. K., M. C. Pant and B. N. Dewan, 1978: Influence of the Arabian Sea on the Indian summer monsoon. *Tellus*, **30**, 117–125.

Hastenrath, S., and P. J. Lamb, 1980: On the heat budget of hydrosphere and atmosphere in the Indian Ocean. *J. Phys. Oceanogr.*, **10**, 694–708.

Hess, S. L., 1959: *Introduction to Theoretical Meteorology.* Holt, Rinehart and Winston, 362 pp.

Hudson, H. R., 1971: On the relationship between horizontal moisture convergence and convective cloud formation. *J. Appl. Meteor.*, **10**, 755–762.

Krishnamurti, T. N., and H. N. Bhalme, 1976: Oscillations of a monsoon system. Part I: Observational aspects. *J. Atmos. Sci.*, **33**, 1937–1954.

——, J. Molinari and H. L. Pan, 1976: Numerical simulation of the Somali jet. *J. Atmos. Sci.*, **33**, 2350–2362.

——, Y. Ramanathan, H.-L. Pan, R. J. Pasch and J. Molinari, 1980: Cumulus parameterization and rainfall rates: I. *Mon. Wea. Rev.*, **108**, 465–472.

Kuo, H. L., 1974: Further studies on the influence of cumulus convection on large-scale flow. *J. Atmos. Sci.*, **31**, 1232–1280.

Lowe, P. R., 1977: An approximation polynomial for the computation of saturation vapor pressure. *J. Atmos. Sci.*, **16**, 100–103.

O'Brien, J. J., 1970: Alternate solutions to the classical vertical velocity problem. *J. Appl. Meteor.*, **9**, 197–203.

Palmen, E., and C. W. Newton, 1969: *Atmospheric Circulation Systems.* Academic Press, 369–522.

Pisharoty, P. R., 1965: Evaporation from the Arabian Sea and the Indian southwest monsoon. *Proc. Symp. on Meteorological Results, 110E,* Bombay, WMO, 43–54.

Pruppacher, H. R., and J. D. Klett, 1978: *Microphysics of Clouds and Precipitation.* D. Reidel, 27–45.

Rao, G. V., W. R. Schaub, Jr. and J. Puetz, 1981: Evaporation and precipitation over the Arabian Sea during several monsoon seasons. *Mon. Wea. Rev.*, **109**, 364–370.

Saha, K. R., 1970: Air and water transport across the equator in western Indian Ocean during northern summer. *Tellus*, **22**, 681–687.

——, and S. N. Bavadekar, 1973: Water vapor budget and precipitation over the Arabian Sea during the northern summer. *Quart. J. Roy. Meteor. Soc.*, **99**, 273–278.

——, and ——, 1977: Moisture flux across the west coast of India and rainfall during the southwest monsoon. *Quart. J. Royal Meteor. Soc.*, **103**, 370–374.

Stout, J. E., D. W. Martin, and D. N. Sikdar, 1979: Estimating GATE rainfall with geosynchronous satellite images. *Mon. Wea. Rev.*, **107**, 585–598.

Thompson, R. M., S. W. Payne, E. E. Recker and R. J. Reed, 1979: Structure and properties of synoptic-scale wave disturbances in the intertropical convergence zone of the eastern Atlantic. *J. Atmos. Sci.*, **36**, 53–72.

Wylie, D. P., and B. B. Hinton, 1981: The feasibility of estimating wind fields for the summer MONEX using cloud motion and ship data. *Bound.-Layer Meteor.*, **21**, 357–367.

Young, J. A., H. Virji, D. P. Wylie and C. Lo, 1980: *Summer Monsoon Windsets from Geostationary Satellite Data.* SSEC, University of Wisconsin-Madison, 127 pp.